Digitalization of scanning lidar measurement campaign planning

Nikola Vasiljević[1], Andrea Vignaroli[1], Andreas Bechmann[1], and Rozenn Wagner[1]
[1]Technical University of Denmark - DTU Wind Energy, Frederiksborgvej 399, Building 118-VEA, 4000 Roskilde, Denmark
Correspondence: Nikola Vasiljević (niva@dtu.dk)

Abstract. By using multiple wind measurements when planing wind farm sites it is possible to decrease the uncertainty of wind farm energy yield assessments since the extrapolation distance between measurements and wind turbines locations are reduced. A WindScanner system consisting of two synchronized scanning lidar potentially represents a cost-effective solution for multi-point measurements, especially in complex terrain. However, the system limitations and limitations imposed by the wind farm site are detrimental to the installation of scanning lidars and the number and location of the measurement positions. To simplify the process of finding suitable measurement positions and associated installation locations for the WindScanner system we have devised a campaign planning workflow. The workflow consists of four phases. In the first phase, based on a preliminary wind farm layout, we generate optimum measurement positions using a greedy algorithm and a measurement 'representative radius'. In the second phase, we create several Geographical Information System (GIS) layers of information such as exclusion zones, line-of-sight (LOS) blockage, and lidar range maps. These GIS layers are then used in the third phase to find optimum positions of the WindScanners with respect to the measurement positions considering the WindScanner measurement uncertainty and logistical constraints. In the fourth phase, we optimize and generate a trajectory through the measurement positions by applying the traveling salesman problem (TSP) on these positions. The above-described workflow has been digitalized into the so-called Campaign Planning Tool (CPT) currently provided as a Python library which allows users an effective way to plan measurement campaigns with WindScanner systems. In this study, the CPT has been tested on three different sites characterized by different terrain complexity and wind farm dimensions and layouts. The CPT shows instantly whether the whole site can be covered by one system or not.

1 Introduction

The development of a wind farm project begins with an assessment of the wind resources and the energy yield for the planned wind farm. Best practices recommend estimating wind resources based on local wind measurements (MEASNET, 2016). Measurement campaigns designed for wind resource assessment have historically relied on anemometers and wind vanes mounted on tall meteorological masts with the goal to measure a wind climate similar to the wind climate the wind turbines will experience during their lifetime. The local measurements are used to produce the observed wind climate of the site.

To account for the seasonal and inter-annual variations of the wind the observed wind climate is long-term corrected using long-term reference data from a nearby meteorological station, reanalysis data or meso-scale models (Carta et al., 2013). The long-term corrected wind climate is then extrapolated vertically and horizontally, typically using a flow model such as WAsP (Mortensen et al., 2014) to estimate the wind resource at hub height for every wind turbine location.

The single mast approach is affordable but can cause large uncertainties. Specifically, in complex terrain (mountainous and forested areas), the spatial extrapolation becomes challenging as the topography can significantly influence the flow. The ideal scenario would be to measure the local wind climate at every planned wind turbine position. However, erecting as many masts as wind turbines would be extremely costly and in some areas impossible.

Many large wind farm projects in complex terrain are developed using multiple masts. Combining one fixed mast and one or several roaming profiling lidars moved to different positions during the campaign is another option. The advantage of roaming vertical profiling lidars lies in their ability to provide affordable high altitude measurements, ease of deployment and absence of building-permits in comparison to the masts, while data availability and inaccuracy in complex terrain (Bingöl et al., 2009) are some of their disadvantages. However, any roaming setup brings a trade-off between the number of measurement positions and the measurement duration at each location since short measurements (e.g. of 3 months) can lead to erroneous wind climate (Langreder and Mercan, 2016).

A potential solution for multi-point measurements for wind resource assessment lies in the application of scanning lidars (Krishnamurthy et al., 2013). With a measurement range of several kilometers and a beam that can be oriented freely in any direction (Vasiljevic et al., 2016), many measurement positions can be reached without moving the hardware. Especially dual-Doppler setups (i.e., two scanning lidars) can provide accurate retrieval of horizontal wind speed and wind direction (i.e., two dimensional (2D) wind vector) at many possible positions (Vasiljević et al., 2017). While scanning lidars provide a broad range of benefits, there are also clear challenges when designing multi-lidar measurement campaigns.

Constraints which arise from scanning lidars, atmosphere and site characteristics dictate the design process mentioned above. Indeed, the beam of scanning lidars can be steered freely, but on the other hand, it can be blocked in some directions by the terrain, vegetation or other obstacles (e.g., power lines). This impacts the positioning of scanning lidars since we need an unobstructed passage of the beams towards measurement points, i.e. clear line-of-sights (LOS). On the other hand, the lidar characteristics (e.g., laser wavelength and output power) in combination with the atmosphere characteristics (e.g., aerosol extinction, backscatter coefficient, and atmospheric attenuation) impact the maximum expected range of the lidar. Furthermore, retrieving the 2D wind vector requires a limited beam elevation angle (e.g., smaller than 5° suggested by Vasiljević et al. (2017)) to avoid contamination of horizontal wind components with the vertical component, finally the intersecting angle of the beams at the measurement points should be large enough (e.g., bigger than 30° suggested by Vasiljevic and Courtney (2017)) to minimise the lidar measurement uncertainty (Davies-Jones, 1979; Stawiarski et al., 2013). Overall, a campaign planner has to handle several constraints at the same time to find the best measurement locations and in accordance with them generate the best possible measurement campaign layout.

In this paper, we describe a workflow and resulting digital tool (named Campaign Planning Tool, CPT) which tackle the above-described challenges involved in the planning of scanning lidar campaigns. The workflow is based on the application

of the methodology for multi-lidar experiments on wind resource assessment campaigns (Vasiljević et al., 2017), which was previously used in planning of more than 20 measurement campaigns (Vasiljevic, 2018) and especially those conveyed in the New European Wind Atlas (NEWA) project (Mann et al., 2017), such as Perdigao-2015 (Vasiljević et al., 2017) and Perdigao-2017 (Fernando et al., 2019). On the other hand, the CPT has previously been conceptualized during the WindScanner.eu project (see 'WindScanner locator' in Vasiljevic and Hasager, 2015).

The paper is organized as follows. Section 2 describes the workflow and corresponding elements of CPT. In Section 3 we present results of applying CPT for planning campaigns at three sites. We discuss the results and future work in Section 4, while we provide our concluding remarks in Section 5.

2 Methodology

2.1 Overview

We assume that the location and the layout of the wind farm are known. These initial information are inputs to the campaign planning workflow which consists of four sequential phases graphically represented in Figure 1. First of all, the measurement positions are optimized based on the wind farm layout. Afterwards, the measurement positions are used in combination with lidar and site constraints to generate the map that highlights best lidar installation locations. In the next phase, the positions of the scanning lidars are determined by minimizing a dual-Doppler measurement uncertainty of horizontal wind speed while identifying existing road and power infrastructure. Finally, considering the measurement positions and positions of scanning lidars the trajectory of the laser beams through all the reachable measurement points is optimized and afterwards generated. In the sections that follow each phase will be described in details followed by a short summary how the entire workflow has been digitalized and thus converted into the CPT.

2.2 Phase 1 - Measurement positions optimization

The wind farm layout is a required input for the campaign planning workflow. For small wind farms (either a limited number of turbines and-or a limited spatial extent) we can coincide the measurement positions with the wind turbine positions. For larger wind farms, the number of measurement points needs to be reduced. However, the reduced set of measurement points should be adequately distributed over the wind farm site to avoid long wind resource extrapolation distances. The simplest approach is to group the wind turbine locations, which are close to each other in clusters, and to assign a single measurement location per cluster. MEASNET (2016) suggests that measurements from a single location represent the wind climate over a certain area described by 'representativeness radius' (R_r). R_r has different values for different terrain types. For example, in complex terrain, the radius should be smaller than 2 km as suggested by MEASNET (2016). By solving a disc covering problem (e.g., Biniaz et al., 2017), in which we aim to find a minimum number of discs with a radius equal to R_r that cover all locations of wind turbines, we cluster the wind turbines and optimize the measurement locations. As stated in Ghasemalizadeh and Razzazi

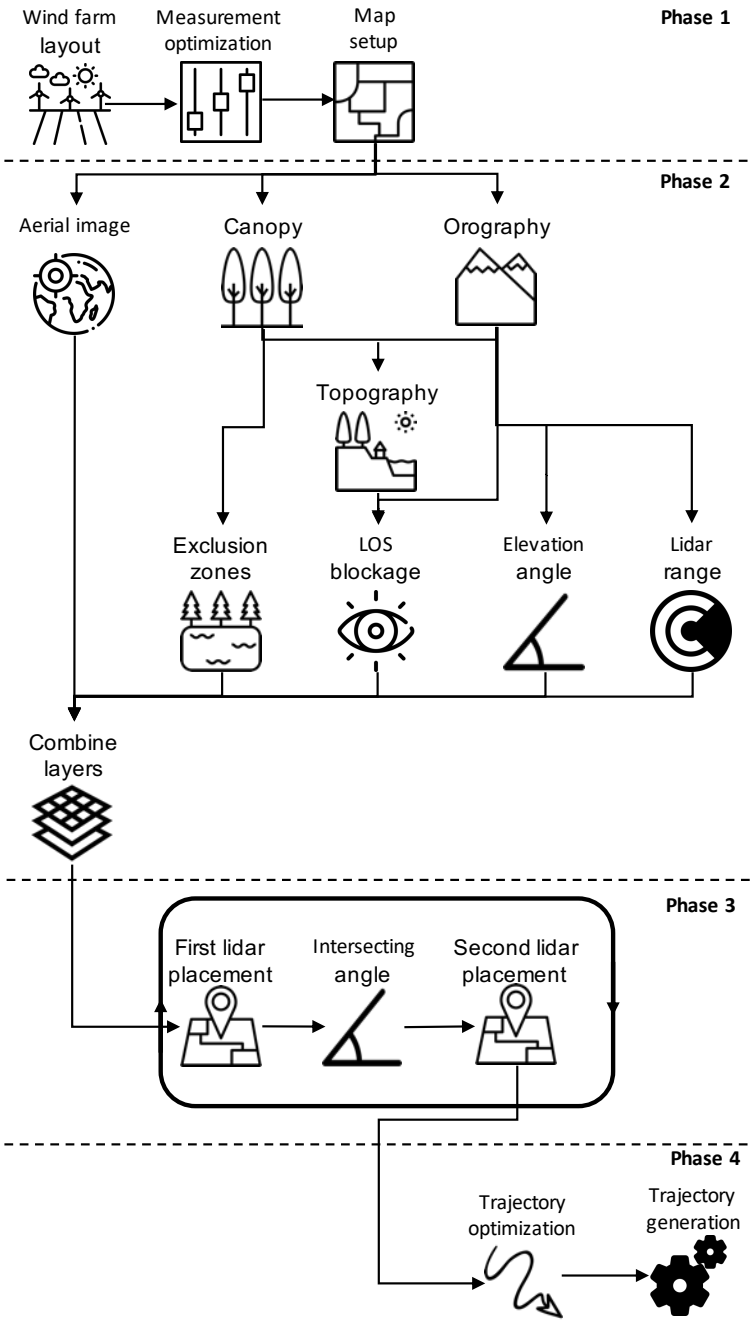

Figure 1. Campaign planning workflow (figure designed using freepik.com icon database)

(2012) there are several ways in solving disc covering problem. One of them is a greedy approach which we adapted to suite our purpose.

In our case, the greedy algorithm implementation yields the set D of m unique disks with the radius R_r covering the set T of n wind turbine positions (T = { T_1,T_2,...,T_n }). We are solving the disc covering problem in two dimensions (2D) by omitting height coordinate (i.e., z) of turbine positions. The greedy algorithm implementation can be described in the algorithmic sense with following steps:

1. Initialize the set D ($D = \emptyset$)

2. For any unique pair of wind turbine positions (there is $p = \frac{n!}{2(n-2)!}$ unique pairs) calculate a midpoint, which is considered as a potential disc center and add it to the set M = { M_1,M_2,...,M_p }

3. Find the elements of the set T that are covered by each element of the set M and form an additional set S which will contain these information. To do this, calculate the distance between each element of the two sets:

$$d_{i,j} = \|M_i - T_j\| = \sqrt{(x_{M_i} - x_{T_j})^2 + (y_{M_i} - y_{T_j})^2}$$
$$i = 1,...,p \quad \wedge \quad j = 1,...,n \tag{1}$$

   where x_m, y_m, x_t and y_t are coordinates of disc centers and turbine positions, and compare $d_{i,j}$ to R_r ($d_{i,j}$ <= R_r condition must be satisfied for a disc M_i to cover a point T_j). Through the comparisons the set S is formed. The elements of S are actually sets themselves containing wind turbine positions covered by each disc from the set M. If for example, a disc M_k covers turbine positions T_1, T_2 and T_n (i.e., $d_{k,1}$, $d_{k,2}$ and $d_{k,n}$ are smaller or equal to R_r) the corresponding element of the set S, that is S_k will contain these elements (i.e., S_k = { T_1, T_2 and T_n }). Alternatively, if a disc M_k does not cover any turbine position the corresponding element of the set S will be an empty set (i.e., $S_k = \emptyset$).

4. Select a disc from the set M which covers the maximum number of points of the set T (this process is aided using the set S). Let this disc be M_i.

5. The disc M_i is added to D and removed from M:

$$D = D \cup M_i \tag{2}$$
$$M = M \cap M_i \tag{3}$$
$$S = S \cap S_i \tag{4}$$

6. Points covered by M_i provided in S_i are removed from the set T and from any subset of the set S:

$$T = T \cap S_i \tag{5}$$
$$\forall S_j \in S, \quad S_j = S_j \cap S_i \tag{6}$$

7. Steps 1 to 6 are repeated until either the set T or S are empty :

$$T = \emptyset \quad \vee \quad S = \emptyset \tag{7}$$

8. If T is not an empty set after Step 7, then the remaining elements are added to the set D :

$$D = D \cup T \tag{8}$$

At the end of this process elements of the set D, that is measurement points, contain only x and y coordinates. Using the digital elevation model (DEM) from the Shuttle Radar Topography Mission (SRTM, Farr et al. (2007)) we can attach the height information to the elements of the set D. It is important to additionally add the hub height of future wind turbines to these height information. As the last step of the first phase we generate a mesh of equally spaced points over the site with the measurement point in the mesh center (see Figure 2). Lets denote the mesh as G and treat it as a set of elements $G_{i,j}$ ($G_{i,j}$ = $\{ x_i, y_j \}$, where i=j=1, ..., l). The mesh resolution should be equal to the land cover and terrain data resolution which will be used in the second phase (typically $|x_2 - x_1|$ = $|y_2 - y_1|$ =100 m). This avoids any interpolation of the land cover or topography datasets to our mesh.

2.3 Phase 2 - Highlighting best lidar installation locations

In this phase we will create a Geographical Information System (GIS) layer which includes site and lidar constraints while highlighting the best lidar installation locations. We will denote this GIS layer as the combined layer and treat it as a set Cl containing elements $Cl_{i,j}$. To create this layer, first we acquire land cover data, orthography data and aerial image corresponding to the extent of the previously generated mesh (Figure 2). For land cover data we can use CORINE Land Cover dataset. In case of the orography, the previously mentioned SRTM DEM datasets serves this purpose, while for the aerial image we can use the Google map server. All three data sources are publicly available. The acquired stack of data will be a base material for the combined layer creation.

At present we consider 5 types of constraints which are detrimental for a lidar installation: zones where a lidar cannot be installed (e.g., lakes, forests, etc.); topographical features that can block the beam; keeping the lidar elevation angle below a certain threshold to avoid measurement contamination with the vertical component of the wind; the maximum lidar range; practical matters such as access roads. To create the combined layer which contains all the above-listed constraints, first we will generate GIS layers for each individual constraint and afterwards merge them. These individual GIS layers are: (1) Exclusion zones layer, (2) LOS blockage layer, (3) Elevation angle layer, (4) Lidar range layer and (5) Logistical layer.

To create the exclusion zone layer we will use the land cover data and according to the land cover type (e.g., water surface, forest, etc.) classify areas of the site as suitable or not for a lidar installation. The land cover data can be treated as a set Lc equally spaced elements $Lc_{i,j}$ containing integer values which represent so-called CLC codes that indicate the land cover type (e.g., water bodies have CLC code from 40 to 44). To generate the exclusion zone layer we make a copy of the mesh (an empty mesh), walk through the mesh (going from one mesh point to another), fetch the corresponding information on land cover type

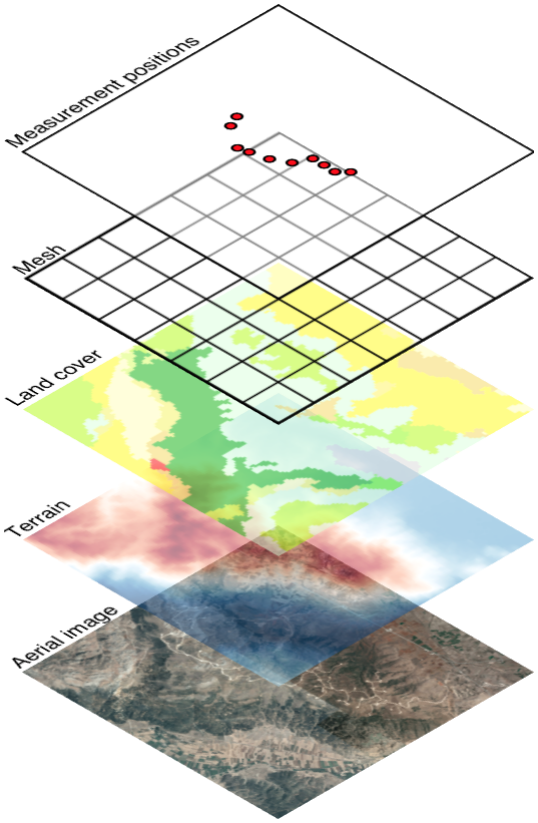

Figure 2. A stack of data used to generate the GIS layer for lidar placement: (1) measurement positions generated by solving disc covering problem, (2) mesh covering wind farm site, (3) land cover data sourced from CORINE Land Cover database, (4) terrain data sourced from SRTM DEM database and (5) aerial image sourced from the Google Map server

from the land cover dataset, check the type and assign value of 1 or 0 to the mesh point if the land cover type allows lidar installation or not (e.g., $G_{i,j}$ ={ x_i, y_i, 1} if CLC code is equal to 12 that is 'Arable land'). An example of a fictive exclusion zone layer is shown in Figure 3.

To generate the LOS blockage layer we need to create dataset contain summed height of the terrain and canopy. To do this we will add 20 m at each location in the DEM dataset where the CORINE Land Cover dataset contains code which correspond to the forest (CLC code equal to 23, 24 and 25). Afterwards, we make a copy of the mesh, walk through the mesh, fetch the corresponding elevation from the DEM dataset, perform a viewshed analysis (Izraelevitz, 2003) from the selected mesh point to each measurement point that returns which measurement points are visible, and assign the visible measurement points to the mesh point (e.g., if measurement points D_1,D_2 and D_n are visible from $G_{i,j}$ then $G_{i,j}$ ={x_i, y_i, D_1, D_2, D_n}). In the viewshed analysis for the selected mesh point we are only taking the corresponding height from the DEM dataset (since we consider that a lidar will be installed on ground), while for the points in between the mesh and measurement points we are

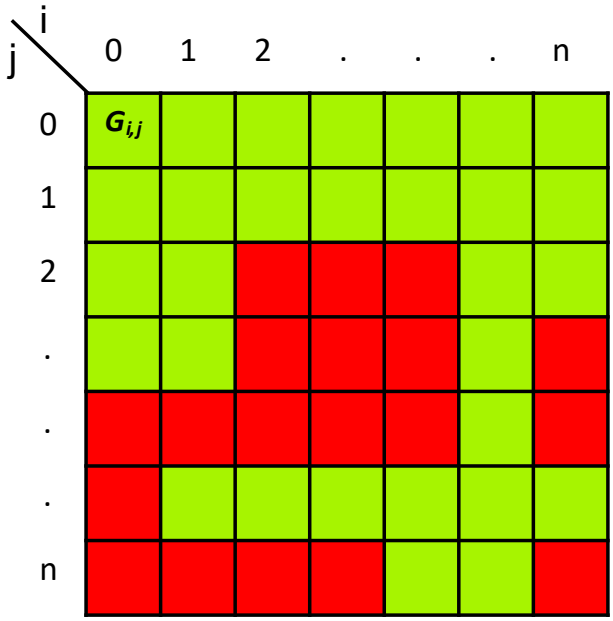

Figure 3. Fictive exclusion zone layer represented as an array: $G_{i,j}$ denotes one mesh point, red and green squares indicate bad ($G_{i,j}$ = 0) and good ($G_{i,j}$ = 1) locations for a lidar installation respectively, i corresponds to x coordinate or Easting and j corresponds to y coordinate or Northing.

considering the summed height dataset. The result of this process is the LOS blockage layer which mesh points contain a set of measurement points to which there is an unobstructed LOS.

As mentioned, our focus is to design a dual-Doppler measurement campaign in order to retrieve the horizontal wind speed. Accordingly, a low elevation beam angle is required to avoid contamination of the LOS speed measurement with the vertical component of the wind vector. We create the elevation angle layer to serve this purpose. This layer is created through following steps: we make a copy of the mesh, walk through each mesh point, fetch the height information from the DEM dataset, calculate the elevation angle from the mesh point to each measurement point, compare the calculated angle to a threshold value (e.g., a maximum of 5° suggested by Vasiljević et al. (2017)), and assign measurement points to the mesh point for which the elevation angle is below the threshold value.

In the lidar range layer mesh points contain measurement points which are within reach of the lidar taking into account the expected range of the lidar for the given site. The layer is created in a similar fashion like the previous one.

To create the combined layer, we will treat the four previously derived layers as sets Ez (exclusion zone layer), Lb (LOS blockage layer), Ea (elevation angle layer) and Lr (lidar range layer). Since each set is made using the same mesh, each set contains the same number of elements. The combined layer, treated as a set Cl containing elements $Cl_{i,j}$, is derived as following:

$$Cl = \{Cl_{1,1}, Cl_{1,2}, ..., Cl_{l,l}\} \tag{9}$$

$$Cl_{i,j} = \begin{cases} \{x_i, y_j, \{\}\}, & \text{if } Ez_{i,j} = \{x_i, y_i, 0\} \\ Lb_{i,j} \cap Ea_{i,j} \cap Lr_{i,j}, & \text{if } Ez_{i,j} = \{x_i, y_i, 1\} \end{cases} \tag{10}$$

Therefore, the mesh points of the combined layer will contain which and how many measurement points are reachable considering the first four above described constraints.

Finally, the aerial image of the site (the logistical layer) is kept separate, it will serve the important purpose of identifying existing road and power infrastructure.

2.4 Phase 3 - Placement of the lidars

The combined layer together with underlying aerial image highlights the 'best' locations for the placement of individual lidars considering all the above-described constraints. However, designing the campaign for a dual-Doppler system, where beams from two lidars need to synchronously cross at every measurement positions, adds one more constraint: the limitation on the beams intersection angle. The measurement uncertainty of a dual-Doppler system increases when the intersecting angle between the laser beam gets small (see Vasiljevic and Courtney (2017)). Therefore the position of the second lidar is very much determined by the position of the first lidar. Considering that we have chosen the first lidar location using the combined layer and the logistical layer, now we need to calculate an additional layer to which we will refer as the intersecting angle layer. This layer is created as following: we make a copy of the mesh, walk through each mesh point considering each mesh point as a second lidar position, calculate intersecting angles between the two laser beams at each measurement point, and add those measurement points to the mesh point for which the intersecting angle is bigger than a specific value (e.g., at least 30° suggested by (Davies-Jones, 1979; Vasiljevic and Courtney, 2017)). Lets treat this GIS layer as a set Ia with elements $Ia_{i,j}$. To highlight the best locations for the second lidar installation the intersecting angle layer should be intersected with the combined layer, i.e. :

$$Sl = Cl \cap Ia \tag{11}$$

where Sl is a set corresponding to the newly created GIS layer for the second lidar placement. The process of selecting a position for the first lidar, followed with the generation of the layer for locating the second lidar and selection of the second lidar position should be performed several times to generate several potentials experiment designs, since only during a field visit it will be possible to determine the most likely design for the measurement campaign. Once the second lidar position is determined, we derive a set of reachable measurement points Dr by both lidars which is actually a subset of the set D ($Dr \in D$).

2.5 Phase 4 - Trajectory optimization and generation

The fourth phase consists of the optimization of the path through the measurement points and the generation of the corresponding trajectory.

In the previous phases, we derived the measurement locations and dual-Doppler campaign layout(s). A next task is to optimize the path through those positions such that the motion of the scanner heads required to steer the beams takes the least amount of time (i.e., increasing sampling rate). One way to achieve this is to adapt the solution for the traveling salesman problem (TSP). In the regular TSP, the goal is to find the shortest path through a set of n cities that a traveling salesman needs to visit. There are multiple approaches to solve the TSP (Reinelt, 1994). One of the simplest implementation of the TSP solution is Nearest Neighbor Heuristics (NNH). As stated in (Reinelt, 1994): *This heuristic for constructing a traveling salesman tour is near at hand. The salesman starts at some city and then visits the city nearest to the starting city. From there he visits the nearest city that was not visited so far, etc., until all cities are visited, and the salesman returns to the start.*

In our case, we have a single set of measurement points D_c which needs to be simultaneously visited by the two laser beams. Since typically two scanning lidars will not be symmetrically positioned with respect to the measurement points we will have two different sets of steering angles D_{s1} and D_{s2} corresponding to the first and second lidar respectively which enable 'visiting' the measurement points with the laser beams. Therefore, we cannot directly apply the above described heuristics. The TSP NNH solution needs to be adapted.

Lets consider that the set D_c is defined as:

$$D_c = \{D_{c,1}, D_{c,2}, ..., D_{c,n}\}, D_{c,i} = \{x_i, y_i, z_i\} \tag{12}$$

while D_{s1} and D_{s2} are defined as:

$$D_{s1} = \{D_{s1,1}, D_{s1,2}, ..., D_{s1,n}\}, D_{s1,i} = \{\theta_{1,i}, \varphi_{1,i}\} \tag{13}$$

$$D_{s2} = \{D_{s2,1}, D_{s2,2}, ..., D_{s2,n}\}, D_{s2,i} = \{\theta_{2,i}, \varphi_{2,i}\} \tag{14}$$

additionally we will make a set I which will contains indexes of the sets' elements:

$$I = \{1, 2, ..., j, ..., n\} \tag{15}$$

The adapted TSP NNH solution for dual-Doppler trajectory can be described in the algorithmic sense with following steps:

1. Initialize empty sets T_{l1} and T_{l2} ($T_{l1} = T_{l2} = \emptyset$), which will contain ordered elements of the optimized trajectory.
2. Select an arbitrary index j from the set I.
3. Set an element l to j ($l = j$).
4. Select elements $D_{s1,l}$ and $D_{s2,l}$.

5. Add the elements $D_{s1,l}$ and $D_{s2,l}$ to the set T_{l1} and T_{l2} respectively, and remove index j and elements $D_{s1,l}$ and $D_{s2,l}$ from the set I, D_{s1} and D_{s2} respectively:

$$T_{l1} = T_{l1} \cup D_{s1,l} \tag{16}$$

$$T_{l2} = T_{l2} \cup D_{s1,2} \tag{17}$$

$$I = I \cap j \tag{18}$$

$$D_{s1} = D_{s1} \cap D_{s1,l} \tag{19}$$

$$D_{s2} = D_{s2} \cap D_{s2,l} \tag{20}$$

6. Calculate sets $\Delta\alpha_1$ and $\Delta\alpha_2$ which contains elements $\Delta\alpha_{1,il}$ and $\Delta\alpha_{2,il}$ (i takes values from the set I), defined as:

$$\Delta\alpha_{1,il} = \{\mid \theta_{1,i} - \theta_{1,l} \mid, \mid \varphi_{1,i} - \varphi_{1,l} \mid\}$$
$$i = 1, 2, ..., n \tag{21}$$

$$\Delta\alpha_{2,il} = \{\mid \theta_{2,i} - \theta_{2,l} \mid, \mid \varphi_{2,i} - \varphi_{2,l} \mid\}$$
$$i = 1, 2, ..., n \tag{22}$$

that describe relative angular moves for the two lidars from the measurement point described by the last element of the sets T_{l1} and T_{l2} (i.e., $D_{s1,l}$ and $D_{s2,l}$ respectively) to all remaining measurement points described by elements of D_{s1} and D_{s2}.

7. Form a set B containing maximum concurring elements of the sets $\Delta\alpha_1$ and $\Delta\alpha_2$:

$$B = \{max(\Delta\alpha_{1,1l}, \Delta\alpha_{2,1l}), max(\Delta\alpha_{1,2l}, \Delta\alpha_{2,2l}), ...,$$
$$max(\Delta\alpha_{1,1n}, \Delta\alpha_{2,1n})\} \tag{23}$$

8. Find index j of an element of the set B which has lowest value.

9. Repeat steps 3 to 8 until the sets D_{s1} and D_{s2} are empty (D_{s1}=D_{s2}= $\emptyset$).

The main modifications of a standard TSP NNH solution is the addition of Step 7 which secures that the trajectory will be optimal for both lidars instead of only one. The difference between the standard and adapted TSP NNH solution can seen from an example shown in Figure 4.

To get the lidars to actually follow the optimized trajectory, we need to describe the motion of the scanners as a function of time. In other words, we need to 'attach' the time component of the trajectory to the spatial description we yielded in the previous steps. When calculating the timing for the trajectory, we assume that the lidars will stop at each measurement point and sample wind speed before they continue to the next measurement points. Therefore, we expect that lidars will perform

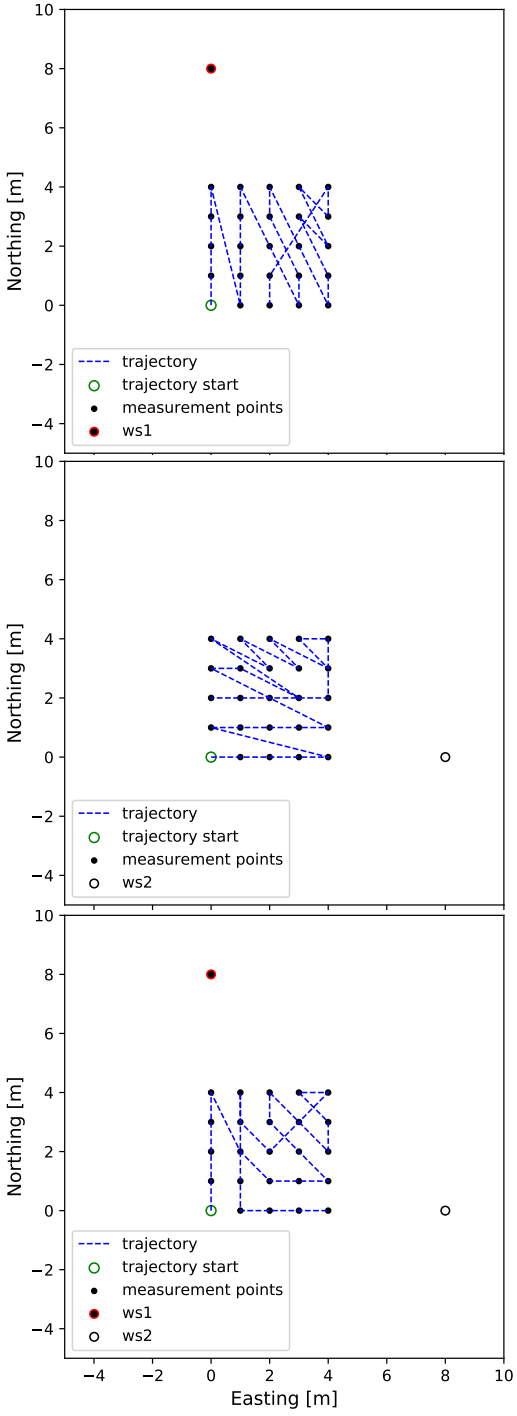

Figure 4. TSP NNH: top image - standard TSP NNH for lidar $ws1$, mid image - standard TSP NNH for lidar $ws2$, bottom image - adapted TSP NNH for two lidars $ws1$ and $ws2$

so-called step-stare trajectories. There are several reasons for selecting step-stare trajectories instead of continuously scanning the flow through the trajectory described by the measurement points. The most important reason is that the current commercial scanning lidars allow only step-stare implementation of complex trajectories. Also, the timing for the step-stare scans can be calculated using a simple solution for Kinematics Elevator Problem (KEP) (e.g., Al-Sharif, 2014) considering an infinite jerk:

$$T_{move} = 2 * \sqrt{\frac{\Delta\beta}{A_{max}}} \tag{24}$$

where T_{move} is a minimum time required to perform an angular motion $\Delta\beta$ considering a maximum allowed acceleration of the lidar scanner head A_{max}.

Since we have two lidars that move to from one to another measurement point, we will generally have two different moving times to perform angular motions. To keep the lidar measurements in sync we take the maximum of the two derived values.

2.6 Campaign planning tool

The previously described workflow has been digitalized resulting in the Campaign Planning Tool (CPT). The CPT is developed in Python in order to be an open source solution which does not require commercial products to be used, improved and further developed. The tool is modular allowing end users to build their own workflows. For example, considering that the installation locations of lidars are predetermined one can recombine modules to find where measurements can be taken followed with the trajectory optimization and generation. At time of writing this manuscript, the tool contains 16 modules where each module is depicted as an icon in Figure 1. Currently, a public release of the tool on a dedicated GitHub (https://github.com/recast-reduced-assesment-time/campaign-planning-tool) is scheduled for the autumn 2019.

3 Results

3.1 Overview

In this section, the campaign planning workflow is demonstrated through the application of CPT on three different wind farm sites, which are named by their country of origin: Scotland (Vasiljevic and Bechmann, 2019a), Italy (Vasiljevic and Bechmann, 2019b) and Turkey (Vasiljevic and Bechmann, 2019c). The only information needed for each site is the wind turbine positions and their hub height. This input could be generated arbitrarily, but to make the examples realistic actual operating wind farms have been chosen. For all three sites, we aim to design the campaign for the long-range WindScanner system configured in a dual-Doppler mode (i.e., the system will have two scanning lidars). The system is described in details in Vasiljevic et al. (2016). To demonstrate the workflow, the most essential bits of information is the maximum range of the lidars, which is 6 km, and maximum acceleration of the scanner heads, which is $100°/s^2$. Results which will be described in the following sections are accessible as a data collection (Vasiljevic et al., 2019) or as an individual datasets (Vasiljevic and Bechmann, 2019a, b, c).

3.2 Site 1 - Scotland

The Scottish site consists of 22 wind turbines with 47-m hub-heights and has a quite compact layout (Figure 5). The distance between adjacent turbines is about 300 m (5 rotor diameters). The wind farm is placed on a 300-m tall hill surrounded by rolling hills of farmland with windbreaks and patches of forest. The hill is quite steep with maximum slopes of 20% from the main south-western wind direction. The site is located 17 km from the coast and can, therefore, be considered an inland site.

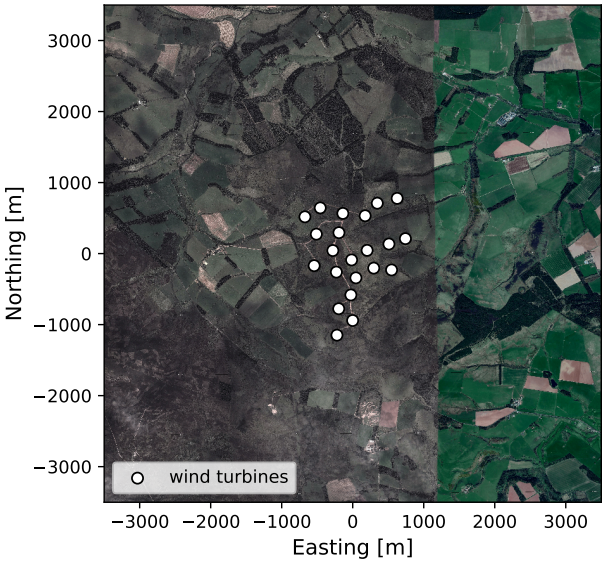

Figure 5. The aerial image of the Scottish site

Due to the compact design of the wind farm, we decided to skip the measurement position optimization and try to generate a measurement campaign in which we intend to measure at every wind turbine position. Considering that the site is relatively close to the coast, surrounded by agricultural land, and the altitude is about 300 m above sea level (asl.), thus relatively low, the site should experience a good concentration of aerosols. Nevertheless, we cannot expect that the WindScanners will have 6 km range all the time and assume that on average the WindScanners would have a range of at least 3 km at the selected site (i.e., a half of the maximum claimed range). This estimation is based on our experience in doing measurement campaigns at various locations and in different atmospheric conditions.

Using this range together with the map extent, the CPT tool outputs the combined layer (see top image in Figure 6). The dark red color areas show positions from where an individual scanning lidar can reach out to all measurement positions. Those areas are relatively large because the wind farm layout is compact. For the purpose of this example, we chose to place the first WindScanner at the South of the wind farm (coordinates of 100 m, -1600m and 400 m in Easting, Northing and altitude asl. respectively relative to the map center coordinates of 535662 m, 6183892 m in Easting and Northing, UTM zone 30 U).

As explained in Section 2 (Phase 3), the first lidar placement is instrumental for the second lidar placement because of the intersecting angle between the respective lidars' beams. There is only one area of the map where the placement of the second lidar assures that all measurement points are within reach and measurable with fair accuracy (bottom image in Figure 6). By selecting the position of the second lidar (coordinates of 1600 m, 400 m and 318 m in Easting, Northing and altitude asl. respectively relative to the map center coordinates), we complete the generation of one measurement campaign layout. In practice, we would generate several layouts (for different positions of WindScanner 1 and WindScanner 2), and assess their feasibility by inspecting aerial images, e.g. looking for access roads and nearby power lines or houses. However, for the sake of demonstrating the workflow, we have generated only a single layout.

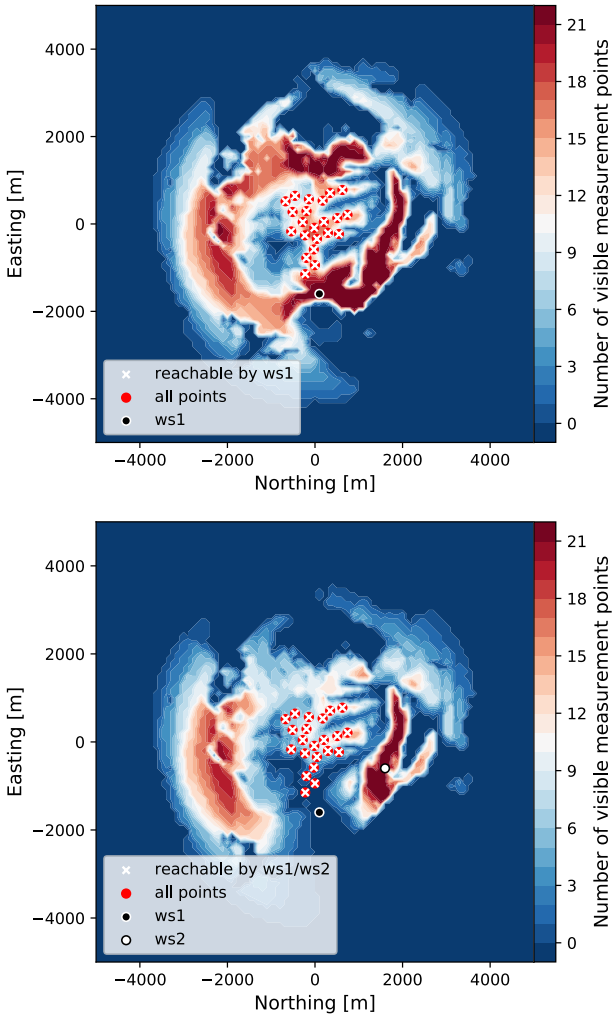

Figure 6. Placing lidars at the Scottish site: top image - locating first lidat at the combined layer, bottom image - locating second lidar at the second lidar placement layer

Since we have both the measurement and lidar positions, we have all the elements to optimize and generate the trajectory. Figure 7 shows the optimum trajectory through the measurement points, resulting from the modified TSP (see Section 2 - Phase 4).

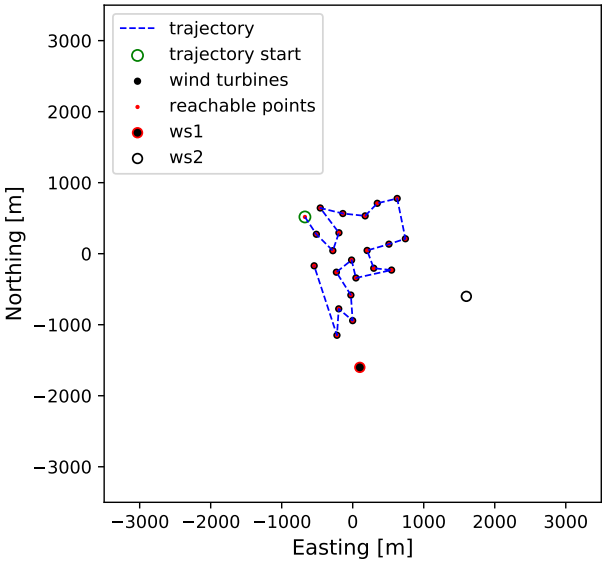

Figure 7. Final campaign design at Scottish site

Considering the kinematic limits of the scanner head and that we are performing step-stare scans, we can apply the elevator kinematic problem on the trajectory points. This step yields the required time to move the scanner heads from one point of the trajectory to another, which in our case is about 14 s for the entire trajectory with additional 22 s for measurements (consult table in Vasiljevic and Bechmann (2019a)). Overall, one complete scan of all measurement points will take about 36 s, which results in about 16 samples of each measurement point per 10-min period. Typically we aim at having at least ten samples per 10-min period which is satisfied with this configuration.

3.3 Site 2 - Italy

The Italian wind farm consists of 36 wind turbines with a 78-m hub-height. The turbines are distributed over a large area (see Figure 8) but somehow clustered in small groups (Figure 13) often with inter-turbine distances of less than 300 m (3 rotor diameters). With a coastline only 10 km to the West, a complex coastal-inland wind climate transition is expected to occur across the wind farm. The terrain has an average 7% slope from the coast to the wind farm. The wind farm is surrounded by farmland, though in a range of about 7 km there are several medium-size towns forming an urban area ring around the farm site.

Given the specific layout of the wind farm, having more or less isolated groups of tightly packed wind turbines, we decided to apply the measurement point optimization. For this wind farm, the representativeness radius was set to 500 m, which is four

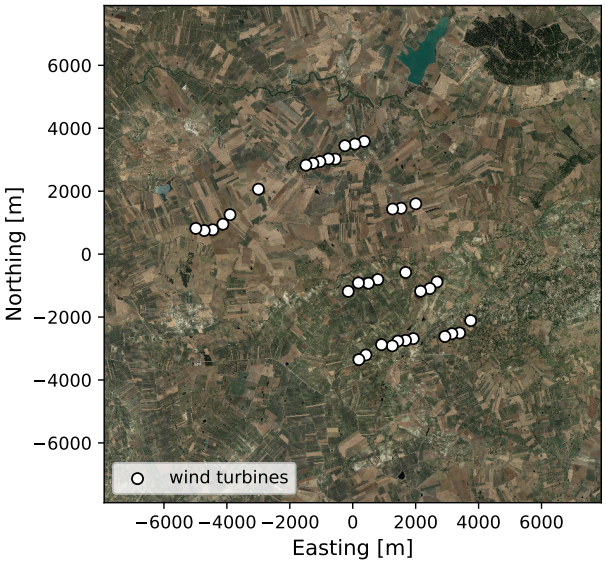

Figure 8. The aerial image of the Italian site

times smaller than the value suggested for the complex terrain sites (MEASNET, 2016). With this conservative setting, the optimization routine found 13 discs of radius equal to 500 m which covers all 36 wind turbine locations (Figure 13). The disc centers are measurement positions.

From there, the workflow was applied in the same way as it was for the Scottish site. In comparison to the Scottish site, the Italian wind farm is even closer to the sea, and it is surrounded by an urban area that in our experience increases the aerosol concentration resulting in an improved lidar range. Therefore, for the Italian site, we can expect to have an average measurement range of 4 km for the WindScanners. The combined layer generated by the CPT is shown as the top image in Figure 10. For this site, there are actually no positions from which any lidar can reach all 13 measurement positions. At best, there are only two locations from which one lidar can reach 11 out of 13 measurement points. The top image of Figure 10 shows the selected location for the first lidar installation (coordinates of -910 m, -640 m and 227 m Northing, Easting and height asl. respectively relative to the map center coordinates of 297200 m and 4189966 in Northing and Easting respectively, UTM zone 33 S).

The layer for the second lidar placement (the bottom image in Figure 10) shows that the second lidar can only reach 7 measurement positions at most and this can only be achieved from a few locations. Of these locations, we selected one which assures that we cover the largest extent of the wind farm, thus getting good spatial information on the farm wind resources. The coordinates of a selected location for the second lidar are 1600 m, 110 m and 278 m in Northing, Easting and height asl. relative to the map center coordinates (the bottom image in Figure 10).

Considering the positions of WindScanners, reachable measurement points, and kinematic limits, we derived an optimum trajectory through the measurement points and calculated the timing for the synchronized scanner head motions (Figure 11).

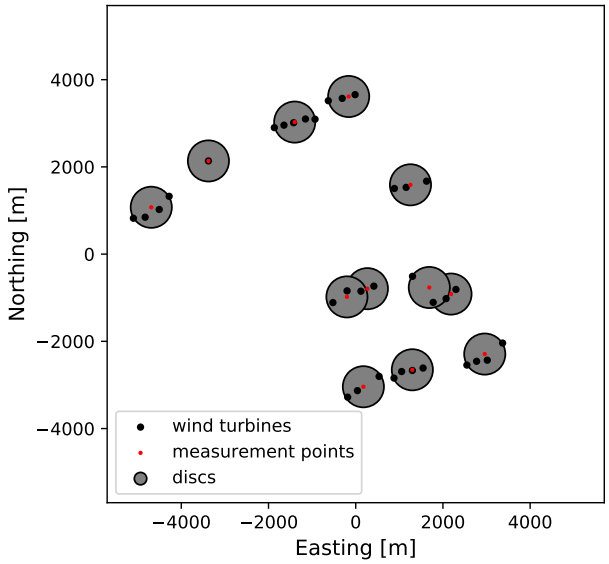

Figure 9. Measurement locations for Italian site: black dots - wind turbine positions, red circles - discs covering wind turbine positions, green dots - optimized measurement positions (i.e., discs' centers)

Based on the calculated timing for the scanner heads motion and considering one second accumulation time per measurement point, one scan through all the points takes roughly 21 s of which 7 s are spent on measurements (consult table in Vasiljevic and Bechmann (2019b)). This provides us with about 28 measurement samples at each measurement point within a 10-min period.

3.4 Site 3 - Turkey

The Turkish wind farm consists of 22 wind turbines with a 80-m hub-height. The wind farm extends 8 km from North to South (see Figure 12) with the three most northerly turbines separated by about 2 km from the rest. The inter-turbine distance is 400-500 m (4-5 rotor diameters) for most turbines. The turbines are located along a 1600 m tall North-South ridge and the main wind direction from North-East (i.e., perpendicular to the ridge line). In the main wind direction the mean terrain slopes are about 12% and with extremes reaching 50% the site should be regarded as very complex. The land cover is sparse vegetation with a patch of forest along Western facing slopes.

For this site, we assumed the average lidar measurement range to be 3 km, and we used the representativeness radius of 500 m. Our assumption on the average range in case of the Turkish site is probably closer to what a lidar would probably achieve in field operation (thus less conservative) due to operation in high altitude where we usually experience low aerosol concentration and often low clouds and fog. On the other hand, the selected representative radius is 100 m lower than in the case of the Italian site, thus about 5 times smaller than the recommended value by MEASNET. Running the workflow using these parameters we

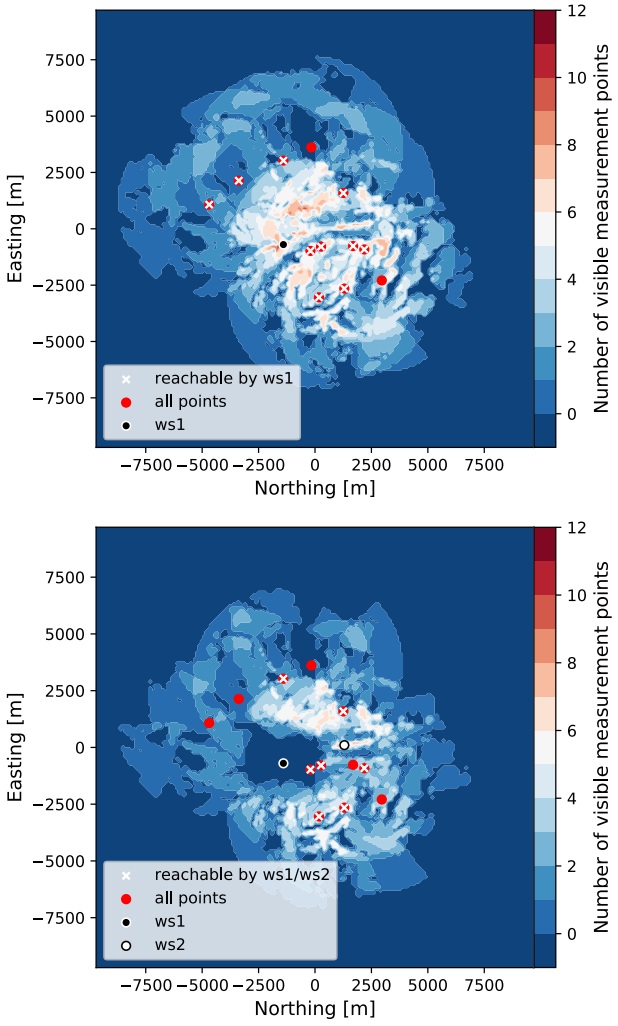

Figure 10. Placing lidars at Italian site: top image - locating first lidat at the combined layer, bottom image - locating second lidar at the second lidar placement layer

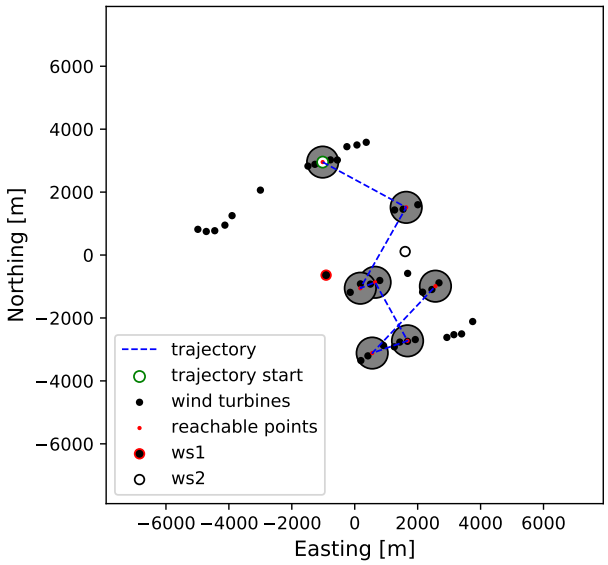

Figure 11. Final campaign design for Italian site

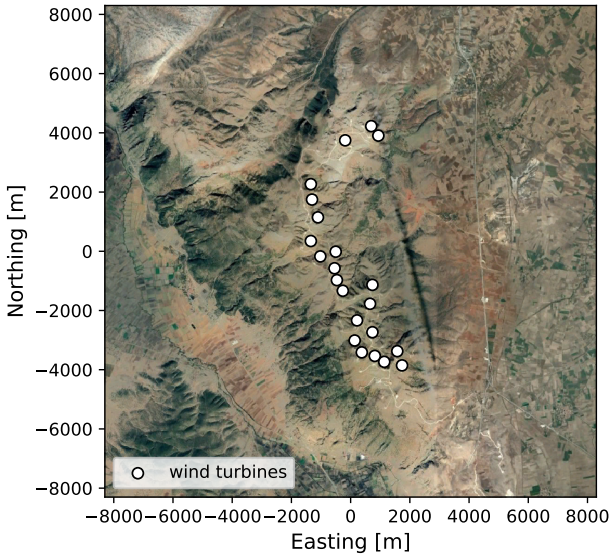

Figure 12. The aerial image of the Turkish site

generate a measurement layout with 10 measurement positions (see Figure 13) with the associated combined layer for the first lidar placement shown in Figure 14, top image.

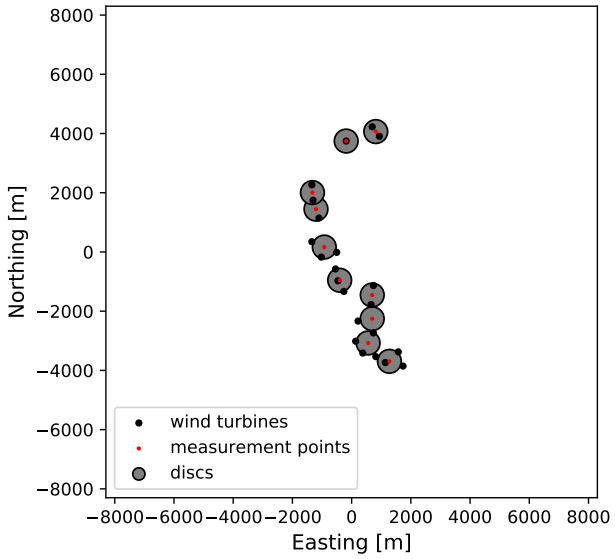

Figure 13. Measurement locations for the Turkish site: black dots - wind turbine positions, red circles - discs covering wind turbine positions, green dots - optimized measurement positions (i.e., discs' centers)

Like for the Italian site case there are only a few locations for placing the two lidars, especially for two inter-dependent reasons one being the wind farm length (8 km) and second being the average range (3 km). Once again the best solution is to place the lidars in the middle of the wind farm. The top image of Figure 14 shows the first lidar placement, which coordinates are -1900 m, -800 m and 1497 m in Northing, Easting and height asl. respectively relative to the map center coordinates (Easting 249626 m and Northing 4227308 m, UTM zone 36 S).

Knowing the first lidar position leads us to the generation of the second lidar placement layers. From the bottom image in Figure 14 there is only a narrow area in the middle of the wind farm where the second lidar could be placed. Also, the bottom image in Figure 14 shows the result of our choice for the second lidar placement (second lidar coordinates are -400 m, -300 m and 1569 m in Northing, Easting and height asl. relative to the map center).

The designed WindScanner layout can provide measurements in 6 out of 10 measurement points which cover the middle part of the wind farm (Figure 15). The upper and lower quarter of the wind farm area are not reachable with the current layout. In principle, we would probably need two WindScanner systems to cover the entire wind farm (i.e., four scanning lidars). Considering the WindScanners and measurement locations together with the kinematic limits as the input for the last phase of the workflow we reach the optimized trajectory which total time is 16 s of which 6 s are spent on the wind speed measurements. This trajectory would provide us with about 35 samples of each measurement point within a 10-min period.

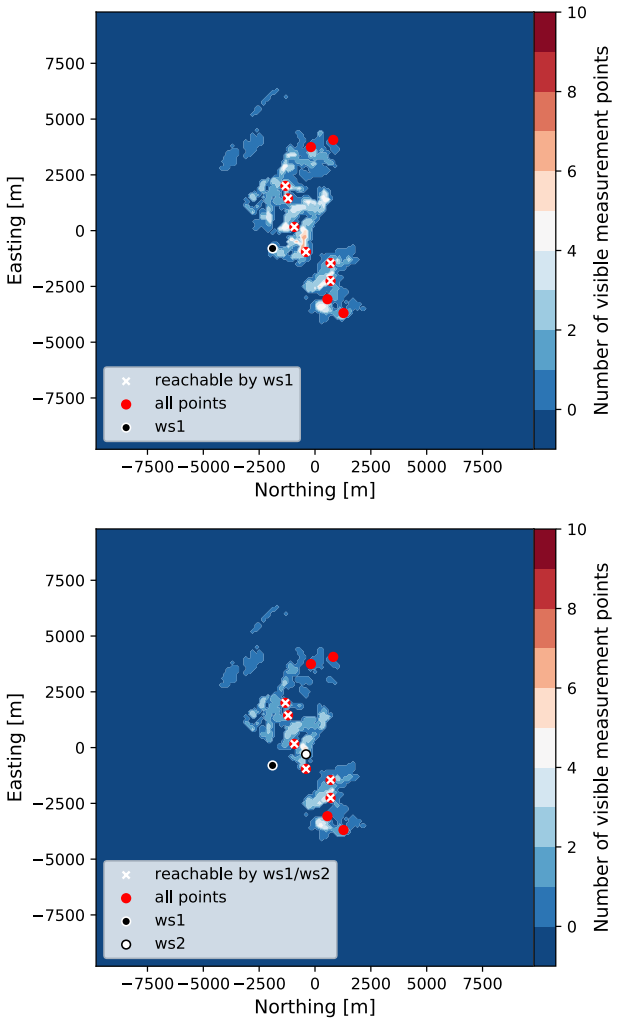

Figure 14. Placing lidars at the Turkish site: top image - locating first lidat at the combined layer, bottom image - locating second lidar at the second lidar placement layer

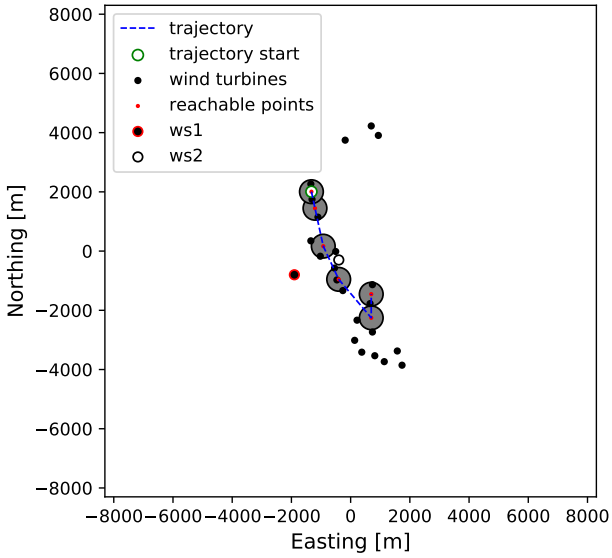

Figure 15. Final campaign layout for Turkish site

4 Discussion

4.1 Discussing results

The primary purpose of the described workflow and corresponding CPT tool up to date is to design a measurement campaign for wind resource assessment (WRA) using a long-range WindScanner system (Vasiljevic et al., 2016) configured in a dual-Doppler mode. This scope follows the RECAST project ambition which is focused on developing a new way of measuring the wind over a site for resource assessment, based on multiple measurement points using WindScanners. This has driven the choice of examples for Section 3 of this paper. However, the workflow and CPT described in this paper are not limited to only planning WRA campaigns. It can be used to design any campaign using one or several scanning lidars. It can easily be applied to any type of scanning lidars since it only requires lidar specifications, which are maximum lidar range and scanner head kinematic limits (i.e., maximum acceleration).

Planning the measurement campaign thoroughly especially with such complex instruments as scanning lidars ensures higher data availability during the campaign and eventually saves time and money. Lidars are very mobile and allow agile measurement campaigns compared to a met mast, but too often the ease of deployment is mistaken with a limited (underestimated) need of planning. This study and the CPT, in general, show the main constraints to lidar measurements in complex terrain and give a practical solution by providing the most suitable positions where the lidar can be placed.

The point of this tool is also to carefully consider the relevance or value of using scanning lidars for a measurement campaign. In the example of the Scottish site, it is relevant to question how much improvement measuring at all turbine positions makes for such a small wind farm. Is it worth using a WindScanner system instead or in addition to one met mast if we compare costs

versus uncertainty in horizontal and vertical extrapolation? One way to trade off for costs is to use scanning lidars for a short period, less than the 12 months required by best practices. The challenge then is the long term correction of the measurement and the related uncertainty.

This study has shown that, for a large site like the Italian or Turkish examples, one set of two WindScanners cannot measure over the whole wind farm area. This is very important to realize at the campaign planning stage when there is still time to either give priority to one part of the site or consider using a second set of two WindScanners to cover the rest of the site.

Another major constraint that must be considered before the lidars deployment is the access roads to or near the lidar locations and possible access to a power source (e.g. existing houses, wind turbines). This is the purpose of the Satellite image used as background for the various GIS layer produced by the CPT.

In order to get around those very strong constraints, as already mentioned, it is, in any case, recommended to generate several campaign designs and to make a site visit with thorough inspection of the possible lidar positions and verification that the data used in the CPT were accurate and up to date (e.g. obstacles, tree height).

4.2 Improving workflow

The presented workflow and developed tool (CPT) can already solve many important challenges regarding the scanning lidar deployment. Nevertheless, we envisage the development of several additional modules which will improve the workflow and the developed tool.

In the current application of CPT, we were predicting the lidar range based on our experience. We plan to extend the 'Lidar range' module to be able to predict the lidar range by developing a lidar simulator. The lidar simulator will take inputs from external databases of global atmospheric visibility or aerosol optical depth for a given site and predict the expected lidar range. In mean time, our suggestion when planning the lidar campaign is to generate campaign layouts considering a conservative approach in which the expected range of the lidar should be in the range between 75 % to 50 % of the claimed range by the lidar manufacturers.

Directly connected to the range prediction is the development of a module which will predict the lidar data availability at any desired range during the planned measurement period. This module will take inputs such as the predicted range from the Lidar range module as well as the cloud height, fog or mist occurrence from the WRF model to predict the data availability.

Furthermore, the module for optimizing measurement positions will be extended by considering other criteria for finding measurement positions apart from the representativeness radius. These are for example terrain elevation, speed-up factors, roughness changes, local obstacles, etc. In principle, we will strive to incorporate anything that can cause local changes in the flow. In other words, the optimization of measurement positions will consider drivers of flow model uncertainty when finding measurement positions.

Finally, we intend to develop an eye safety module that will produce yet another restriction zone (GIS) layer for the placement of lidars. The module will impose geometrical limitations when designing campaign layout to avoid that the laser beam is steered over the site at a height where we could expect that the human eyes can be directly exposed to it.

5 Conclusions

In this paper, we have provided an exhaustive description of the workflow we recommend for planning measurement campaigns using scanning lidars or WindScanner systems. The purpose is to find the most suitable positions for the lidars given the measurement positions, the characteristics of the site (topography), the characteristics of the lidars (measurement range, kinematic limits) and the position of the two lidars relative to each other. The workflow is available through a Python library, named the Campaign Planning Tool, which will be made public during the RECAST project. The CPT has been demonstrated for planning campaigns for resource assessment on three different sites. For a small wind farm layout, the WindScanners could be placed so that measurements could be made at all turbine positions. For the other sites, that were larger, the number of measurement points was needed to be optimized and a set of two lidars could only cover some part of the site. In any case, it is recommended to generate several possible campaign layouts and to make a site visit to take the final decision.

The CPT is easy and fast and helps to design realistic lidar measurement campaigns. Measurement campaigns are costly and risky, especially when using advanced measurement technology. The CPT helps to avoid many pitfalls that can be predicted before the start of the campaign, limiting the risks to the campaign itself.

Data availability. Data described in Section 3 of the paper are available as a data collection at https://doi.org/10.11583/DTU.c.4559624.v1

Author contributions. Conceptualization, N.V., A.V., A.B. and R.W.; Methodology, N.V. and A.V.; Software, N.V. and A.V.; Validation, N.V.; Formal Analysis, N.V.; Investigation, N.V. and A.V.; Resources, N.V. and A.B.; Data Curation, N.V.; Writing - Original Draft, N.V., A.B., R.W. and A.V.;Writing - Review & Editing, N.V., A.B., R.W. and A.V; Visualization, N.V.; Project Administration, R.W. and N.V.; Funding Acquisition, R.W. and A.B.

Competing interests. Authors declare no competing interests.

Acknowledgements. The authors would like to acknowledge Morten Thøgersen (EMD) for his support during the conceptualization phase of the study described in the paper. The financial support for the study has been provided by the RECAST project, which is funded by Innovation Fund Denmark (7046-00021B).

References

Al-Sharif, L.: Intermediate Elevator Kinematics and Preferred Numbers (METE III), Lift Report, 40, 20–31, https://www.researchgate.net/publication/275408222_Intermediate_Elevator_Kinematics_and_Preferred_Numbers_METE_III, 2014.

Bingöl, F., Mann, J., and Foussekis, D.: Conically scanning lidar error in complex terrain, Meteorologische Zeitschrift, 18, 189–195, 2009.

Biniaz, A., Liu, P., Maheshwari, A., and Smid, M.: Approximation Algorithms for the Unit Disk Cover Problem in 2D and 3D, Comput. Geom. Theory Appl., 60, 8–18, https://doi.org/10.1016/j.comgeo.2016.04.002, https://doi.org/10.1016/j.comgeo.2016.04.002, 2017.

Carta, J. A., Velázquez, S., and Cabrera, P.: A review of measure-correlate-predict (MCP) methods used to estimate long-term wind characteristics at a target site, 27, 362–400, https://doi.org/10.1016/j.rser.2013.07.004, https://linkinghub.elsevier.com/retrieve/pii/S1364032113004498, 2013.

Davies-Jones, R. P.: Dual-Doppler Radar Coverage Area as a Function of Measurement Accuracy and Spatial Resolution, Journal of Applied Meteorology, 18, 1229–1233, https://doi.org/10.1175/1520-0450-18.9.1229, 1979.

Farr, T. G., Rosen, P. A., Caro, E., Crippen, R., Duren, R., Hensley, S., Kobrick, M., Paller, M., Rodriguez, E., Roth, L., Seal, D., Shaffer, S., Shimada, J., Umland, J., Werner, M., Oskin, M., Burbank, D., and Alsdorf, D.: The Shuttle Radar Topography Mission, Reviews of Geophysics, 45, https://doi.org/10.1029/2005RG000183, https://agupubs.onlinelibrary.wiley.com/doi/abs/10.1029/2005RG000183, 2007.

Fernando, H., Mann, J., Palma, J., Lundquist, J., Barthelmie, R., BeloPereira, M., Brown, W., Chow, F., Gerz, T., Hocut, C., Klein, P., Leo, L., Matos, J., Oncley, S., Pryor, S., Bariteau, L., Bell, T., Bodini, N., Carney, M., Courtney, M., Creegan, E., Dimitrova, R., Gomes, S., Hagen, M., Hyde, J., Kigle, S., Krishnamurthy, R., Lopes, J., Mazzaro, L., Neher, J., Menke, R., Murphy, P., Oswald, L., Otarola-Bustos, S., Pattantyus, A., Rodrigues, C. V., Schady, A., Sirin, N., Spuler, S., Svensson, E., Tomaszewski, J., Turner, D., van Veen, L., Vasiljević, N., Vassallo, D., Voss, S., Wildmann, N., and Wang, Y.: The Perdigão: Peering into Microscale Details of Mountain Winds, Bulletin of the American Meteorological Society, 0, null, https://doi.org/10.1175/BAMS-D-17-0227.1, https://doi.org/10.1175/BAMS-D-17-0227.1, 2019.

Ghasemalizadeh, H. and Razzazi, M.: An Improved Approximation Algorithm for the Most Points Covering Problem, Theory of Computing Systems, 50, 545–558, https://doi.org/10.1007/s00224-011-9353-4, https://doi.org/10.1007/s00224-011-9353-4, 2012.

Izraelevitz, D.: A Fast Algorithm for Approximate Viewshed Computation, Photogrammetric Engineering Remote Sensing, 69, https://doi.org/10.14358/PERS.69.7.767, 2003.

Krishnamurthy, R., Choukulkar, A., Calhoun, R., Fine, J., Oliver, A., and Barr, K.: Coherent Doppler lidar for wind farm characterization, Wind Energy, 16, 189–206, https://doi.org/10.1002/we.539, https://onlinelibrary.wiley.com/doi/abs/10.1002/we.539, 2013.

Langreder, W. and Mercan, B.: Roaming Remote Sensing - Quantification of Seasonal Bias, in: WindEurope Summit 2016, WindEurope, https://windeurope.org/summit2016/conference/proceedings-Pr0cghyDVy/statscounter2.php?id=2&IDABSTRACT=207, 2016.

Mann, J., Angelou, N., Arnqvist, J., Callies, D., Cantero, E., Arroyo, R., Courtney, M., Cuxart, J., Dellwik, E., Gottschall, J., Ivanell, S., Kuhn, P., Lea, G., Matos, C., Palma, J., Pauscher, L., Peña, A., Rodrigo, J., Söderberg, S., Vasiljevic, N., and Rodrigues, C.: Complex terrain experiments in the New European Wind Atlas, Philosophical Transactions of the Royal Society A: Mathematical, Physical and Engineering Sciences, 375, https://doi.org/10.1098/rsta.2016.0101, 2017.

MEASNET: MEASNET Procedure: Evaluation of Site-Specific Wind Conditions, Version 2, http://www.measnet.com/wp-content/uploads/2016/05/Measnet_SiteAssessment_V2.0.pdf, 2016.

Mortensen, N., Heathfield, D., Rathmann, O., and Nielsen, M.: Wind Atlas Analysis and Application Program: WAsP 11 Help Facility, 2014.

Reinelt, G.: The Traveling Salesman: Computational Solutions for TSP Applications, Springer-Verlag, Berlin, Heidelberg, 1994.

Stawiarski, C., Träumner, K., Knigge, C., and Calhoun, R.: Scopes and Challenges of Dual-Doppler Lidar Wind Measurements—An Error Analysis, Journal of Atmospheric and Oceanic Technology, 30, 2044–2062, https://doi.org/10.1175/JTECH-D-12-00244.1, 2013.

Vasiljevic, N.: (2.5 + 5.8) Years of successes and failures with long-range WindScanner system, https://doi.org/10.5281/zenodo.1442592, https://doi.org/10.5281/zenodo.1442592, 2018.

Vasiljevic, N. and Bechmann, A.: Dual-Doppler measurement campaign design for complex terrain site in Scotland, https://doi.org/10.11583/DTU.8344028.v1, last access: 2019-07-2, 2019a.

Vasiljevic, N. and Bechmann, A.: Dual-Doppler measurement campaign design for complex terrain site in Italy, https://doi.org/10.11583/DTU.8343989.v1, last access: 2019-07-2, 2019b.

Vasiljevic, N. and Bechmann, A.: Dual-Doppler measurement campaign design for complex terrain site in Turkey, https://doi.org/10.11583/DTU.8344061.v1, last access: 2019-07-2, 2019c.

Vasiljevic, N. and Courtney, M.: Accuracy of dual-Doppler lidar retrievals of near- shore winds, https://doi.org/10.5281/zenodo.1441178, https://doi.org/10.5281/zenodo.1441178, 2017.

Vasiljevic, N. and Hasager, C. B.: WindScanner Information System, https://doi.org/10.5281/zenodo.1175211, https://doi.org/10.5281/zenodo.1175211, 2015.

Vasiljevic, N., Lea, G., Courtney, M., Cariou, J.-P., Mann, J., and Mikkelsen, T.: Long-Range WindScanner System, Remote Sensing, 8, https://doi.org/10.3390/rs8110896, http://www.mdpi.com/2072-4292/8/11/896, 2016.

Vasiljević, N., L. M. Palma, J. M., Angelou, N., Carlos Matos, J., Menke, R., Lea, G., Mann, J., Courtney, M., Frölen Ribeiro, L., and M. G. C. Gomes, V. M.: Perdigão 2015: methodology for atmospheric multi-Doppler lidar experiments, Atmospheric Measurement Techniques, 10, 3463–3483, https://doi.org/10.5194/amt-10-3463-2017, https://www.atmos-meas-tech.net/10/3463/2017/, 2017.

Vasiljevic, N., Bechmann, A., Vignaroli, A., and Wagner, R.: Campaign Planning Tool results for three sites in complex terrain, https://doi.org/10.11583/DTU.c.4559624.v2, last access: 2019-07-2, 2019.